Random transition-rate matrices for the master equation

Carsten Timm*
Institute for Theoretical Physics, Technische Universität Dresden, 01062 Dresden, Germany
(Received 22 May 2009; published 31 August 2009)

Random-matrix theory is applied to transition-rate matrices in the Pauli master equation. We study the distribution and correlations of eigenvalues, which govern the dynamics of complex stochastic systems. Both the cases of identical and of independent rates of forward and backward transitions are considered. The first case leads to symmetric transition-rate matrices, whereas the second corresponds to general asymmetric matrices. The resulting matrix ensembles are different from the standard ensembles and show different eigenvalue distributions. For example, the fraction of real eigenvalues scales anomalously with matrix dimension in the asymmetric case.

DOI: 10.1103/PhysRevE.80.021140 PACS number(s): 02.50.−r, 05.40.−a, 02.10.Yn, 05.10.−a

I. INTRODUCTION

The Pauli master equation is encountered in many fields of science such as physics, chemistry, and biology. It describes the time evolution of probabilities for a system to be in certain states. Formally identical rate equations describe the dynamics of concentrations or populations of certain entities. The dynamics of probabilities is described by the Pauli master equation

$$\dot{P}_i = \sum_{j\neq i} (R_{ij}P_j - R_{ji}P_i), \tag{1}$$

where P_i is the probability to find the system in state $i=1,\ldots,N$ and R_{ij} is the transition rate from state j to state i. Evidently, the rates of change in probabilities depend only on the probabilities at time t, i.e., Eq. (1) describes a memoryless or Markovian process. Equation (1) ensures that the total probability is conserved,

$$\frac{d}{dt}\sum_i P_i = \sum_{ij,i\neq j} (R_{ij}P_j - R_{ji}P_i) = 0. \tag{2}$$

Typical applications in physics include lasers [1], disordered conductors [2], microelectronic devices [3], quantum dots [4], and molecular electronics [5]. In these cases one can, in principle, obtain the Pauli master equation by first deriving a *quantum* master equation for the reduced density matrix of a small system, which is obtained by tracing out the reservoir degrees of freedom from the full density operator [6–10]. If the off-diagonal components of the reduced density matrix decay rapidly, it is sufficient to keep only the diagonal components representing the probabilities P_i of states $|i\rangle$ of the small system. In certain fields, for example, in transport and laser theory, the resulting equations [Eq. (1)] are often called *rate equations*.

However, if even the small system is complicated, such as a system of interacting enzymes, this route becomes unfeasible. In applications outside of physics, where i could refer to the state of a technical or social process, a quantum-statistical description becomes inappropriate in any case. One would then view Eq. (1) as the fundamental description.

Our goal is to make progress in the understanding of the master equations for complex systems. The number N of possible states will typically be large. It should be noted that, however, complex behavior can already emerge for moderate N. An example is provided by the differential conductance calculated in Ref. [11] for a magnetic molecule with magnetic anisotropy axis not aligned with the applied magnetic field, where $N=20$; but due to noncommuting terms in the Hamiltonian, many rates are nonzero and are distributed over a broad range.

A. Properties of the master equation

We first recount some basic properties. It is clear that one can rewrite Eq. (1) in the form

$$\dot{P}_i = \sum_j A_{ij}P_j, \tag{3}$$

or $\dot{\mathbf{P}}=A\mathbf{P}$ with the transition-rate matrix, or, for short, rate matrix,

$$A_{ij} \equiv \begin{cases} R_{ij} & \text{for } i\neq j, \\ -\sum_{k\neq j} R_{kj} & \text{for } i=j. \end{cases} \tag{4}$$

It follows that the column sums vanish,

$$\sum_i A_{ij} = 0 \quad \text{for all } j. \tag{5}$$

Note that $(d/dt)\Sigma_i P_i=\Sigma_{ij}A_{ij}P_j$ vanishes for all P_j if and only if Eq. (5) holds. Constraint (5) is thus dictated by conservation of probability. From Eq. (4) it is also clear that

$$A_{ij} \geq 0 \quad \text{for all } i\neq j, \tag{6}$$

if we interpret the R_{ij} as transition rates. A matrix satisfying inequality (6) and $\Sigma_i A_{ij}\leq 0$ for all j is called a *compartmental matrix*.

Equation (3) can be solved by the ansatz $\mathbf{P}=e^{\lambda t}\mathbf{v}$, which leads to the eigenvalue equation $A\mathbf{v}=\lambda\mathbf{v}$. Since A is generally not symmetric, the eigenvalues λ and the components of the right eigenvectors $\mathbf{v}$ can be complex. However, since A is

*carsten.timm@tu-dresden.de

real, the equation $A\mathbf{v}=\lambda\mathbf{v}$ implies $A\mathbf{v}^*=\lambda^*\mathbf{v}^*$. Thus, the eigenvalues are real with real eigenvectors or form complex-conjugate pairs with their eigenvectors also being complex conjugates.

Let $\mathbf{v}_n$ be the right eigenvector to eigenvalue λ_n. It is well known that there is always at least one strictly zero eigenvalue, which we call $\lambda_0=0$: constraint (5) implies that A has a left eigenvector $(1,1,\ldots,1)$ to the eigenvalue $\lambda_0=0$. The corresponding right eigenvector $\mathbf{v}_0$ describes the stationary state.

A real eigenvector $\mathbf{v}_n$ with real eigenvalue λ_n describes a contribution to the probability vector $\mathbf{P}$ that decays exponentially with the rate $-\lambda_n$. A complex-conjugate pair of eigenvectors $\mathbf{v}_n$ and $\mathbf{v}_n^*$ with eigenvalues λ_n and λ_n^* can be combined to form the two independent real solutions $(e^{\lambda_n t}\mathbf{v}_n + e^{\lambda_n^* t}\mathbf{v}_n^*)/2$ and $(e^{\lambda_n t}\mathbf{v}_n - e^{\lambda_n^* t}\mathbf{v}_n^*)/2i$. Writing the components of $\mathbf{v}_n$ as $v_{nj}=v_{nj}^0 e^{i\phi_{nj}}$ with v_{nj}^0 real, we obtain the solutions

$$v_{nj}^0 e^{\mathrm{Re}\,\lambda_n t}\begin{cases}\cos(\mathrm{Im}\,\lambda_n t+\phi_{nj}),\\ \sin(\mathrm{Im}\,\lambda_n t+\phi_{nj}).\end{cases} \tag{7}$$

The initial values at time $t=0$ are clearly Re v_{nj} and Im v_{nj}, respectively. We thus find damped harmonic oscillations with damping rate $-\mathrm{Re}\,\lambda_n$ and angular frequency $\mathrm{Im}\,\lambda_n$. We obtain the solution at all times by expanding the initial probability vector $\mathbf{P}(t=0)$ into the basis of real vectors $\mathbf{v}_n$ (for real λ_n), and Re $\mathbf{v}_n$ and Im $\mathbf{v}_n$ (for complex-conjugate pairs λ_n and λ_n^*).

An eigenvalue λ_n with $\mathrm{Re}\,\lambda_n>0$ would be unphysical since the corresponding contribution to the probabilities would diverge for $t\to\infty$. However, for any compartmental matrix the spectrum is contained in $\{\lambda|\mathrm{Re}\,\lambda<0\}\cup\{0\}$ [12,13]. Thus all eigenvalues are either zero or have a strictly negative real part.

The Perron-Frobenius theorem [14,15] applied to the non-negative matrix $A-a_{\min}I$, where $a_{\min}<0$ is the minimum of A_{ii} and I is the $N\times N$ unit matrix, shows that the right eigenvector $\mathbf{v}_0$ to λ_0 has only non-negative components. This ensures that the probabilities in the stationary state are non-negative.

B. Random rate matrices

As noted above, even relatively simple problems lead to master equations with rates A_{ij}, $i\neq j$, distributed over a broad range. In problems with large numbers of states it is often impractical to obtain all independent components A_{ij}. This situation is reminiscent of Hamiltonians for complex systems. Difficult problems of this type concern atomic nuclei and quantum dots, where the Hamiltonian is too complicated to write down explicitly, but cannot be simplified by methods restricted to weakly interacting systems. For these systems, random-matrix theory (RMT) [16–19] has lead to significant progress. The main assumption is that a Hamiltonian of this type is a typical representative of an ensemble of Hamiltonians of appropriate symmetry. While this approach does not allow one to obtain specific eigenvalues, it does provide information about the statistical properties of the spectrum [16–19].

Our point of departure is to treat the rate matrix A for a complex system as an element of a suitable random-matrix ensemble. In the case of transport through quantum dots, this is complementary to treating the Hamiltonian of the quantum dot as a random matrix, which has been done extensively [17].

Since the rate matrix A must satisfy conditions (5) and (6), we define the *exponential general rate-matrix ensemble* (EGRE): the EGRE is formed by real $N\times N$ matrices A with independently identically distributed off-diagonal components A_{ij} with the distribution function

$$p(A_{ij})=\begin{cases}\dfrac{1}{\langle R\rangle}e^{-A_{ij}/\langle R\rangle} & \text{for } A_{ij}\geq 0,\\ 0 & \text{otherwise},\end{cases} \tag{8}$$

and the diagonal components

$$A_{jj}=-\sum_{i\neq j}A_{ij}. \tag{9}$$

The exponential distribution of rates A_{ij} is viewed as the least biased distribution of non-negative numbers. We will also present results that do not depend on the specific distribution function p. We will see that the specific distribution becomes irrelevant in the limit of large N, at least if all its moments exist. The distribution of components is thus not the most fundamental difference between the EGRE and the well-known ensembles studied in the context of random Hamiltonians. Rather, one such difference lies in constraint (5) or (9). The other is that the rate matrices are real but not symmetric and thus not Hermitian [20].

Ensembles of non-Hermitian matrices have been studied in detail, starting with Ginibre's work on Gaussian ensembles of non-Hermitian matrices with real, complex, and quaternion components [21]. We will compare our results to the real Ginibre ensemble.

To be able to analyze the importance of the asymmetry, we also define the *exponential symmetric rate-matrix ensemble* (ESRE): the ESRE is formed by real symmetric $N\times N$ matrices A with independently identically distributed components A_{ij} above the diagonal $(i<j)$ with the distribution function given by Eq. (8) and the diagonal components given by Eq. (9).

Another possible choice is a two-valued distribution of rates, where a transition from state j to state i is either possible or impossible, and all possible transitions have the same rate. This case with symmetric rates has been studied by various authors [22–24]. It is essentially equivalent to adjacency matrices of random simple networks.

An ensemble of real symmetric matrices satisfying Eq. (5) but with a Gaussian distribution of A_{ij} has also been studied [24]. This case cannot easily be interpreted in terms of a master equation since the A_{ij} can be negative. We will compare our results for the eigenvalue spectrum to these works below.

The remainder of this paper is organized as follows: in Sec. II we consider the simpler case of symmetric rate matrices (the ESRE), and obtain results for the eigenvalue density and for the correlations between neighboring eigenval-

ues. In Sec. III we then study general rate matrices (the EGRE) and obtain results for the eigenvalue density, now in the complex plane, and for the correlations of neighboring eigenvalues. We conclude in Sec. IV. A number of analytical derivations are relegated to Appendixes A through C.

II. SYMMETRIC RATE-MATRIX ENSEMBLE

We first consider ensembles of symmetric rate matrices A. These describe processes where transitions from any state j to state i and from i to j occur with the same rate, $A_{ij}=A_{ji}$.

A. Spectrum

As noted above, the spectrum always contains the eigenvalue $\lambda_0=0$. The corresponding eigenvector for symmetric matrices is $(1,1,\ldots,1)$ or, normalized to unit probability, $(1/N,1/N,\ldots,1/N)$. For symmetric rates, the stationary state is thus characterized by equal distribution over all states i. We are interested in the distribution of the other eigenvalues λ_n, $n=1,\ldots,N-1$, which are all real. We have also seen in Sec. I A that $\lambda_n\leq 0$. Since there is no further constraint, the probability of λ_n for any $n>0$ being exactly zero vanishes.

To simplify the calculations, we shift the matrices so that they have zero mean. We discuss this immediately for general matrices. Also, nothing here depends on the distribution function p of the rates A_{ij}, as long as the average $\langle R\rangle \equiv\langle A_{ij}\rangle$ exists. We define

$$\tilde{A}\equiv A-\langle A\rangle, \tag{10}$$

where, here and in the following, angular brackets denote the average over the matrix ensemble under consideration. Here, $\langle A\rangle$ has the components $\langle A_{ij}\rangle=\langle R\rangle$ for $i\neq j$ and $\langle A_{ii}\rangle =-(N-1)\langle R\rangle$. It follows that $\Sigma_i\tilde{A}_{ij}=0$ for all j. Consequently, $\tilde{A}$ has a left eigenvector $\mathbf{w}_0^T\equiv(1,1,\ldots,1)$ to the eigenvalue $\tilde{\lambda}_0=0$.

Let $\mathbf{v}_n$ be the right eigenvectors of A to the eigenvalues λ_n, $n=1,\ldots,N-1$. Since $\mathbf{w}_0^T$ is the left eigenvector to the eigenvalue $\lambda_0=0$, we have $\mathbf{w}_0^T\mathbf{v}_n=0$. Since

$$\langle A\rangle=\langle R\rangle\begin{pmatrix}1 & \cdots & 1\\ \vdots & \ddots & \vdots\\ 1 & \cdots & 1\end{pmatrix}-N\langle R\rangle I, \tag{11}$$

$\mathbf{v}_n$ is a right eigenvector of $\langle A\rangle$ to the eigenvalue $-N\langle R\rangle$. Therefore, $\mathbf{v}_n$ is also a right eigenvector of $\tilde{A}$ to the eigenvalue $\tilde{\lambda}_n=\lambda_n+N\langle R\rangle$. The result is that the shifted matrices $\tilde{A}$ also have one eigenvalue $\tilde{\lambda}_0=0$ and that the remaining eigenvalues are just the eigenvalues of A, shifted by $N\langle R\rangle$.

We now derive the average of eigenvalues λ_n, here and in the following excluding $\lambda_0=0$. We have $\langle\lambda\rangle'=\langle\tilde{\lambda}\rangle'-N\langle R\rangle$, where angular brackets with a prime denote the average over all eigenvalues, excluding the exact zero. Since this leaves $N-1$ eigenvalues, their average is the trace of the matrix, to which the zero eigenvalue does not contribute, divided by $N-1$. Consequently,

$$\langle\tilde{\lambda}\rangle'=\frac{1}{N-1}\mathrm{Tr}\langle\tilde{A}\rangle=\frac{1}{N-1}\mathrm{Tr}\,0=0, \tag{12}$$

so that

$$\langle\lambda\rangle'=-N\langle R\rangle. \tag{13}$$

This result is independent of the specific distribution function of rates, p, as long as $\langle R\rangle$ exists.

We next calculate the low-order central moments,

$$\mu_m\equiv\langle\tilde{\lambda}^m\rangle'=\langle(\lambda-\langle\lambda\rangle')^m\rangle'=\langle(\lambda+N\langle R\rangle)^m\rangle', \tag{14}$$

of the eigenvalues λ_n, $n>0$. The central moments are identical to the central moments of the shifted values $\tilde{\lambda}_n$. Unless otherwise noted, our results for μ_m hold for an arbitrary distribution function of rates, p, as long as the moments exist. It is instructive to show the calculation of the second moment explicitly. We find

$$\mu_2=\langle\tilde{\lambda}^2\rangle'=\frac{1}{N-1}\mathrm{Tr}\langle\tilde{A}^2\rangle=\frac{1}{N-1}\sum_{ij}\langle\tilde{A}_{ij}\tilde{A}_{ji}\rangle$$

$$=\frac{1}{N-1}\sum_i\left(\sum_{j\neq i}\langle\tilde{A}_{ij}\tilde{A}_{ji}\rangle+\langle\tilde{A}_{ii}\tilde{A}_{ii}\rangle\right). \tag{15}$$

Using $\tilde{A}_{ij}=\tilde{A}_{ji}$ and $\Sigma_k\tilde{A}_{ki}=0$, we obtain

$$\mu_2=\frac{1}{N-1}\sum_i\left(\sum_{j\neq i}\langle\tilde{A}_{ij}^2\rangle+\sum_{k,l\neq i}\langle\tilde{A}_{ki}\tilde{A}_{li}\rangle\right). \tag{16}$$

With $\langle\tilde{A}_{ij}\rangle=0$ we finally get

$$\mu_2=\frac{2}{N-1}\sum_i\sum_{j\neq i}\langle\delta R^2\rangle=2N\langle\delta R^2\rangle, \tag{17}$$

where $\langle\delta R^2\rangle\equiv\langle A_{ij}^2\rangle-\langle A_{ij}\rangle^2$ for $i\neq j$ is the second central moment of $p(A_{ij})$. For the special case of an exponential distribution, we have $\langle\delta R^2\rangle=\langle R\rangle^2$ and thus $\mu_2=2N\langle R\rangle^2$.

The important consequence is that, while the mean of the nonzero eigenvalues of the unshifted matrices A scales with N [Eq. (13)], the width of their distribution is only $\sqrt{\mu_2}=\sqrt{2N\langle\delta R^2\rangle}\propto\sqrt{N}$. Thus for large N the distribution of eigenvalues contains a single eigenvalue $\lambda_0=0$ and the remaining $N-1$ eigenvalues form a narrow distribution around $-N\langle R\rangle$. In physical terms, nearly all deviations from the stationary state decay on the same time scale $1/N\langle R\rangle$.

All moments can be obtained by the same method: we first write the average in terms of a trace, split the sum into terms with equal or distinct matrix indices, and use $\Sigma_k\tilde{A}_{ki}=0$. With $\tilde{A}_{ij}=\tilde{A}_{ji}$ and $\langle\tilde{A}_{ij}\rangle=0$ we obtain the moments. Since the enumeration of all possible cases of equal or distinct indices is cumbersome, we have used a symbolic algebra scheme implemented with MATHEMATICA [25]. The results up to $m=8$ are shown in Table I for a general distribution. The moments are expressed in terms of the central moments $\langle\delta R^n\rangle\equiv\langle(A_{ij}-\langle A_{ij}\rangle)^n\rangle$. Note that in the limit of large N, the moments μ_m for even m only depend on the second moment $\langle\delta R^2\rangle$. We will return to this point shortly.

Table II shows the central moments μ_m up to $m=10$ for the exponential distribution of A_{ij}, $i<j$ (ESRE). For the ex-

TABLE I. Central moments μ_m, $m=2,\ldots,8$, of the nonzero eigenvalues λ for ensembles of symmetric rate matrices. The results hold independently of the distribution function p of rates A_{ij}, $i<j$, as long as the moments exist. Here, $\langle \delta R^n \rangle$ is the nth central moment of p.

m	μ_m (symmetric matrices, general distribution)
2	$2N\langle \delta R^2 \rangle$
3	$-4N\langle \delta R^3 \rangle$
4	$N[9(N-2)\langle \delta R^2 \rangle^2+8\langle \delta R^4 \rangle]$
5	$-2N[25(N-2)\langle \delta R^2 \rangle\langle \delta R^3 \rangle+8\langle \delta R^5 \rangle]$
6	$N[4(14N^2-73N+90)\langle \delta R^2 \rangle^3+73(N-2)\langle \delta R^3 \rangle^2$ $+132(N-2)\langle \delta R^2 \rangle\langle \delta R^4 \rangle+32\langle \delta R^6 \rangle]$
7	$-2N[7(41N^2-211N+258)\langle \delta R^2 \rangle^2\langle \delta R^3 \rangle$ $+203(N-2)\langle \delta R^3 \rangle\langle \delta R^4 \rangle$ $+168(N-2)\langle \delta R^2 \rangle\langle \delta R^5 \rangle+32\langle \delta R^7 \rangle]$
8	$N[(431N^3-4042N^2+12021N-11322)\langle \delta R^2 \rangle^4$ $+6(306N^2-1561N+1898)\langle \delta R^2 \rangle^2\langle \delta R^4 \rangle$ $+593(N-2)\langle \delta R^4 \rangle^2+1088(N-2)\langle \delta R^3 \rangle\langle \delta R^5 \rangle$ $+4(N-2)(507N-1574)\langle \delta R^2 \rangle\langle \delta R^3 \rangle^2$ $+832(N-2)\langle \delta R^2 \rangle\langle \delta R^6 \rangle+128\langle \delta R^8 \rangle]$

ponential distribution, one has $\langle \delta R^n \rangle = !n\langle R \rangle^n$, where $!n \equiv n!\Sigma_{k=0}^{n}(-1)^k/k!$ is the subfactorial. Table II also contains the leading large-N terms for the ESRE. At least up to $m=10$, the even moments scale as $\mu_m \sim N^{m/2}$ for large N, as expected from the scaling of μ_2. However, the odd moments scale only as $\mu_m \sim N^{(m-1)/2}$. If this holds for all m, the distribution of $\tilde{\lambda}$ approaches an even function for large N. This is indeed the case, as we shall see.

The density of eigenvalues $\tilde{\lambda}_n$ can be obtained from the resolvent [26] $\tilde{G}(z) \equiv (z-\tilde{A})^{-1}$. The density is given by the spectral function

TABLE II. Second column: central moments μ_m, $m=2,\ldots,10$, of the nonzero eigenvalues λ for ensembles of symmetric rate matrices, assuming an exponential distribution of rates (ESRE). Third column: leading term of μ_m for large N.

m	μ_m (ESRE)	μ_m (ESRE, $N \gg 1$)
2	$2N\langle R \rangle^2$	$2N\langle R \rangle^2$
3	$-8N\langle R \rangle^3$	$-8N\langle R \rangle^3$
4	$9N(N+6)\langle R \rangle^4$	$9N^2\langle R \rangle^4$
5	$-4N(25N+126)\langle R \rangle^5$	$-100N^2\langle R \rangle^5$
6	$4N(14N^2+297N+1470)\langle R \rangle^6$	$56N^3\langle R \rangle^6$
7	$-4N(287N^2+4046N+20424)\langle R \rangle^7$	$-1148N^3\langle R \rangle^7$
8	$N(431N^3+20594N^2+250576N$ $+1311648)\langle R \rangle^8$	$431N^4\langle R \rangle^8$
9	$-4N(3453N^3+95021N^2+1089414N$ $+5957208)\langle R \rangle^9$	$-13812N^4\langle R \rangle^9$
10	$2N(1971N^4+172657N^3+3737127N^2$ $+42106610N+241175496)\langle R \rangle^{10}$	$3942N^5\langle R \rangle^{10}$

$$\rho_{\mathrm{all}}(z) = -\frac{1}{\pi N}\mathrm{Im}\ \mathrm{Tr}\langle \tilde{G}(z+i\eta)\rangle, \tag{18}$$

where $\eta \to 0^+$ at the end of the calculation. The density includes the exact zero eigenvalue so that we can write

$$\rho_{\mathrm{all}}(z) = \frac{1}{N}\delta(z) + \frac{N-1}{N}\rho(z), \tag{19}$$

where $\rho(z)$ is the normalized density of nonzero eigenvalues. In the limit of large N, the eigenvalue density $\rho_{\mathrm{all}}(z) \cong \rho(z)$ only depends on the second moment $\langle \delta R^2 \rangle$ of the distribution function p of rates, at least as long as all moments of p exist. The proof is sketched in Appendix A. That the eigenvalue distribution generically becomes independent of p for large N has been conjectured by Mehta (conjecture 1.2.1 in Ref. [19]). However, the second part of this conjecture, stating that the density of eigenvalues is the same as for the Gaussian orthogonal ensemble (GOE), is not true for our ensemble.

Since the density of eigenvalues $\tilde{\lambda}_n$, $n>0$, of the shifted matrices $\tilde{A}$ only depends on the second moment $\langle \delta R^2 \rangle$ for large N, we can obtain the large-N behavior from any distribution with that second moment. We choose the Gaussian distribution

$$p_G(\tilde{A}_{ij}) = \frac{1}{\sqrt{2\pi\langle \delta R^2 \rangle}}\exp\left(-\frac{\tilde{A}_{ij}^2}{2\langle \delta R^2 \rangle}\right). \tag{20}$$

For this distribution together with the constraint $\Sigma_i \tilde{A}_{ij}=0$, the eigenvalue density is known for large N [24]: the averaged resolvent is the solution of

$$\langle \tilde{G}(z) \rangle = \frac{1}{\sqrt{N\langle \delta R^2 \rangle}} g\left(\frac{z - N\langle \delta R^2 \rangle\langle \tilde{G}(z)\rangle}{\sqrt{N\langle \delta R^2 \rangle}}\right), \tag{21}$$

where

$$g(z) \equiv \frac{1}{\sqrt{2\pi}}\int_{-\infty}^{\infty} dx \frac{e^{-x^2/2}}{z-x}. \tag{22}$$

This integral can be evaluated,

$$g(z) = \sqrt{\frac{\pi}{2}}z\sqrt{-\frac{1}{z^2}}e^{-z^2/2}\left(-2+\mathrm{erfc}\frac{z^2\sqrt{-1/z^2}}{\sqrt{2}}\right). \tag{23}$$

$g(z)$ has a cut along the whole real axis. The density $\rho(z)$ is thus nonzero for all real z. Equations (18) and (21) imply that $\sqrt{N\langle \delta R^2 \rangle}\rho(z)$ is a universal function of $z/\sqrt{N\langle \delta R^2 \rangle}$. The same distribution in the large-N limit was found for adjacency matrices [22,23]. The corresponding result for the GOE is the well-known semicircle law [16,19]. It is worth pointing out that the different eigenvalue density results only from the constraint $\Sigma_i \tilde{A}_{ij}=0$.

We now study the eigenvalue density for the ESRE for finite N. We perform Monte Carlo simulations by generating a number n_r of realizations of matrices from the ESRE for given N, shifted according to Eq. (10). The matrices are diagonalized and the eigenvalue with the numerically smallest

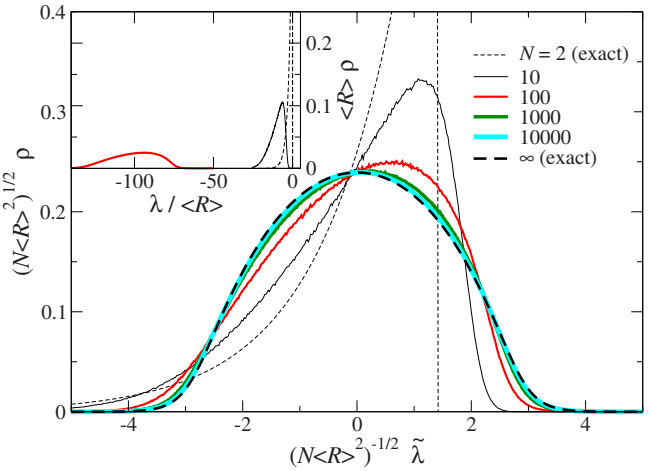

FIG. 1. (Color online) Scaled density of nonzero eigenvalues of shifted symmetric rate matrices $\tilde{A}=A-\langle A\rangle$. The results for $N=2$ and $N\to\infty$ are exact, see text. The curves for $N=10$, 100, 1000, and 10 000 are histograms with 500 bins for 10^7 eigenvalues for matrices randomly chosen from the ESRE. Inset: unscaled distribution of eigenvalues of the unshifted matrices A for $N=2$, 10, and 100.

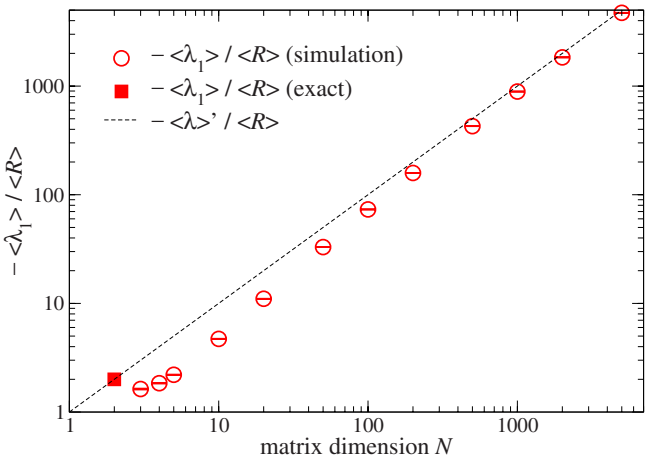

FIG. 2. (Color online) Average smallest in magnitude eigenvalue, $\langle\lambda_1\rangle$, of matrices from the ESRE, as a function of N. The open circles denote numerical results for $n_r=5000$ (1000) realizations for $N\leq 1000$ ($N\geq 2000$). Error bars denoting the statistical errors are shown. The filled square denotes the result $\lambda_1=-2\langle R\rangle$ for $N=2$. The dashed straight line denotes the mean of nonzero eigenvalues, $-N\langle R\rangle$.

magnitude, which corresponds to $\tilde{\lambda}_0=0$, is dropped. The eigenvalues are rescaled according to $\tilde{\lambda}\to\tilde{\lambda}/\sqrt{N\langle\delta R^2\rangle}$. Finally, histograms with 500 bins are generated.

Results for $N=2$, 10, 100, 1000, 10 000, and ∞ are shown in Fig. 1. For $N\to\infty$, we solve Eq. (21). For $N=2$, the matrices have a single nonzero eigenvalue $-2\tilde{A}_{12}$ with distribution following from Eq. (8). For each of the other values of N, $n_rN=10^7$ eigenvalues have been generated. Figure 1 shows that the distribution changes smoothly from shifted exponential for $N=2$ to the known universal function for $N\to\infty$. The inset of Fig. 1 shows the unscaled eigenvalue density of the unshifted ESRE to illustrate that the mean scales with N, whereas the width scales with $\sqrt{N}$.

While we have shown that nearly all nonzero eigenvalues lie in a narrow interval around their mean for large N, the dynamics after a transient will be dominated by the slowest process. The slowest nonstationary process is governed by the eigenvalue $\lambda_1<0$, which is smallest in magnitude. It is conceivable that matrices from the ESRE typically have an eigenvalue λ_1 close to zero. For example, λ_1 could scale with a lower power of N compared to the mean $-N\langle R\rangle$. If the fraction of such anomalously slow rates decreased for large N, they might not be visible in the density plots in Fig. 1.

To check this, we plot the mean $\langle\lambda_1\rangle$ as a function of N in Fig. 2. The average slowest rate $|\langle\lambda_1\rangle|$ is significantly smaller than the average rate $|\langle\lambda\rangle'|$ for small N, as one would expect from the width $\sqrt{\mu_2}\propto\sqrt{N}$. On the other hand, for large N, $|\langle\lambda_1\rangle|$ approaches $|\langle\lambda\rangle'|$. Thus we do not find evidence for anomalously slow processes. Instead, the slowest rate is consistent with the mean and width of the eigenvalue distribution $\rho(\lambda)$.

B. Eigenvalue correlations

Since the eigenvalue density for the ESRE differs significantly from the GOE, one might ask whether the correlations between eigenvalues are also different. In the GOE, the distribution function of differences of neighboring eigenvalues λ and λ' approaches zero as $|\lambda'-\lambda|$ for $\lambda'\to\lambda$.

Figure 3 shows the distribution function $\rho_{\mathrm{NN}}(\Delta\lambda)$ of separations $\Delta\lambda\equiv\lambda_{n+1}-\lambda_n$ of neighboring eigenvalues for the ESRE (here, the λ_n are assumed to be ordered by value). The zero eigenvalue $\lambda_0=0$ is excluded. Since the width of the eigenvalue distribution scales as $\sqrt{N}$ while the number of eigenvalues for a given realization scales as N, the typical separation should scale as $1/\sqrt{N}$. We, therefore, rescale $\Delta\lambda\to\sqrt{N/\langle R\rangle^2}\Delta\lambda$. Figure 3 shows that the rescaled distribution approaches a limiting form for $N\to\infty$. Furthermore, the distribution function $\rho_{\mathrm{NN}}(\Delta\lambda)$ is linear in $\Delta\lambda$ for small $\Delta\lambda$ for all N. Thus the distribution of nearest-neighbor separations behaves essentially like for the GOE [19]. Constraint (5),

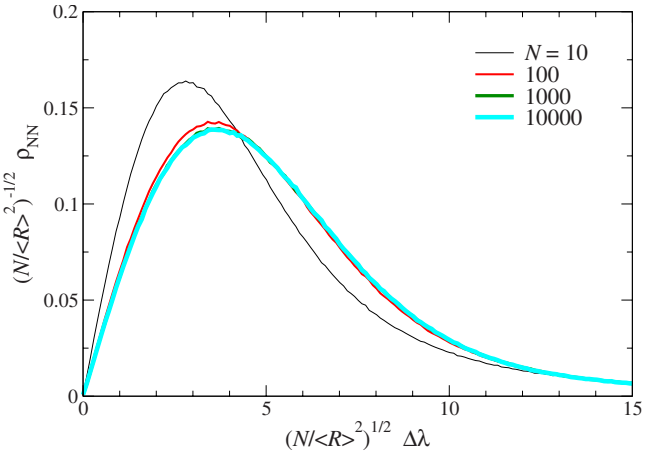

FIG. 3. (Color online) Scaled distribution of nearest-neighbor separations $\Delta\lambda$ of nonzero eigenvalues for the ESRE for $N=10$, 100, 1000, and 10 000, from the same data sets as in Fig. 1. The curve for $N=1000$ is nearly obscured by the one for $N=10$ 000.

which is responsible for the deviation of the eigenvalue distribution from the GOE result, does not have a comparably strong effect on the eigenvalue correlations. The reason is very likely that the joint probability distribution $\rho(\lambda_1,\lambda_2,\ldots,\lambda_{N-1})$ of the eigenvalues [19], while being complicated for the ESRE, does contain the factor $\Pi_{nn',0<n<n'}|\lambda_n-\lambda_{n'}|$, which determines the exponent $\beta=1$ in $\rho_{\mathrm{NN}}\sim\Delta\lambda^{\beta}$.

III. GENERAL RATE-MATRIX ENSEMBLE

We now turn to the ensemble of general, asymmetric rate matrices (EGRE). Compared to the ESRE, it describes the opposite extreme of independent rates A_{ij} and A_{ji} for forward and backward transitions.

A. Spectrum

As noted, there always exists an eigenvalue $\lambda_0=0$ with left eigenvector $(1,1,\ldots,1)$. Other than for the symmetric case, the corresponding right eigenvector is different. We are interested in the distribution of the other eigenvalues λ_n, $n=1,\ldots,N-1$, which are now complex with negative real parts. We have already shown in Sec. II that the mean of nonzero eigenvalues equals $-N\langle R\rangle$, see Eq. (13). We shift the matrices according to Eq. (10) so that they have zero mean.

We define the expectation values

$$\mu_m \equiv \langle\widetilde{\lambda}^m\rangle' = \langle(\lambda-\langle\lambda\rangle)^m\rangle' = \langle(\lambda+N\langle R\rangle)^m\rangle' \tag{24}$$

in analogy to the ESRE but they are not the central moments of the distribution of nonzero eigenvalues. Instead, the central moments have to be defined for a two-dimensional distribution in the complex plane,

$$\mu_{mn} \equiv \langle(\mathrm{Re}\,\lambda+N\langle R\rangle)^m(\mathrm{Im}\,\lambda)^n\rangle'. \tag{25}$$

Since the eigenvalues are real or form complex-conjugate pairs, we have $\mu_{mn}=0$ for odd n. We show in Appendix B that the shifted eigenvalue distribution only depends on the second moment $\langle\delta R^2\rangle$ of p, like we found for the symmetric case. We here call the μ_m in Eq. (24) the *pseudomoments*. They are all real since the eigenvalues are real or form complex-conjugate pairs.

The pseudomoments μ_m can be obtained in the same way as for symmetric matrices. The results are different since $\langle\widetilde{A}_{ij}\widetilde{A}_{ji}\rangle=\langle\delta R^2\rangle$ for the symmetric case, whereas $\langle\widetilde{A}_{ij}\widetilde{A}_{ji}\rangle=0$ for the general case. We present the pseudomoments μ_m up to $m=8$ for a general distribution function $p(A_{ij})$ in Table III and up to $m=10$ for the exponential distribution (EGRE) in Table IV. The scaling of μ_m for even and odd m and large N is the same as for the ESRE. In the limit $N\to\infty$, only the even pseudomoments survive. Interestingly, at least up to $m=10$, these agree with the central moments of a real *Gaussian* distribution, $\mu_m^G=(m-1)!!(N\langle\delta R^2\rangle)^{m/2}$, where $n!!=n(n-2)(n-4)\cdots$ is the double factorial. We show in Appendix C that this identity holds for all even m.

The eigenvalue distribution in the complex plane can be obtained from the nonanalyticities of the averaged resolvent $\langle\widetilde{G}(z)\rangle=\langle(z-\widetilde{A})^{-1}\rangle$ [26,27]. However, unlike for symmetric matrices, the nonanalyticities are not limited to a branch cut along the real axis. For what follows, it is more convenient to employ the method of hermitization [27]. We define the $2N\times 2N$ matrix

$$\mathcal{H}(z,z^*) \equiv \begin{pmatrix} 0 & \widetilde{A}-zI \\ \widetilde{A}^T-z^*I & 0 \end{pmatrix}, \tag{26}$$

where $\widetilde{A}^T$ is the transpose of $\widetilde{A}$. $\mathcal{H}(z,z^*)$ is Hermitian for any complex z. With the resolvent of $\mathcal{H}$,

$$\mathcal{G}(\eta;z,z^*) \equiv \frac{1}{\eta-\mathcal{H}(z,z^*)}, \tag{27}$$

the density of eigenvalues in the complex plane is [27]

TABLE III. Pseudomoments μ_m, $m=2,\ldots,8$, of the nonzero eigenvalues λ for ensembles of general rate matrices. The results hold independently of the distribution function p of rates A_{ij}, $i\neq j$, as long as the moments exist.

m	μ_m (general matrices, general distribution)
2	$N\langle\delta R^2\rangle$
3	$-N\langle\delta R^3\rangle$
4	$N[3(N-1)\langle\delta R^2\rangle^2+\langle\delta R^4\rangle]$
5	$-N[10(N-1)\langle\delta R^2\rangle\langle\delta R^3\rangle+\langle\delta R^5\rangle]$
6	$N[(15N^2-49N+38)\langle\delta R^2\rangle^3+10(N-1)\langle\delta R^3\rangle^2+15(N-1)\langle\delta R^2\rangle\langle\delta R^4\rangle+\langle\delta R^6\rangle]$
7	$-N[21(5N^2-17N+14)\langle\delta R^2\rangle^2\langle\delta R^3\rangle+35(N-1)\langle\delta R^3\rangle\langle\delta R^4\rangle+21(N-1)\langle\delta R^2\rangle\langle\delta R^5\rangle+\langle\delta R^7\rangle]$
8	$N[3(35N^3-240N^2+551N-422)\langle\delta R^2\rangle^4+6(35N^2-121N+102)\langle\delta R^2\rangle^2\langle\delta R^4\rangle+35(N-1)\langle\delta R^4\rangle^2+56(N-1)\langle\delta R^3\rangle\langle\delta R^5\rangle+56(5N^2-18N+16)\langle\delta R^2\rangle\langle\delta R^3\rangle^2+28(N-1)\langle\delta R^2\rangle\langle\delta R^6\rangle+\langle\delta R^8\rangle]$

TABLE IV. Second column: pseudomoments μ_m, $m=2,\ldots,10$, of the nonzero eigenvalues λ for ensembles of general rate matrices, assuming an exponential distribution of rates (EGRE). Third column: leading term of μ_m for large N.

m	μ_m (EGRE)	μ_m (EGRE, $N\gg 1$)
2	$N\langle R\rangle^2$	$N\langle R\rangle^2$
3	$-2N\langle R\rangle^3$	$-2N\langle R\rangle^3$
4	$3N(N+2)\langle R\rangle^4$	$3N^2\langle R\rangle^4$
5	$-4N(5N+6)\langle R\rangle^5$	$-20N^2\langle R\rangle^5$
6	$N(15N^2+126N+128)\langle R\rangle^6$	$15N^3\langle R\rangle^6$
7	$-6N(35N^2+140N+148)\langle R\rangle^7$	$-210N^3\langle R\rangle^7$
8	$N(105N^3+2290N^2+6270N+7476)\langle R\rangle^8$	$105N^4\langle R\rangle^8$
9	$-8N(315N^3+2953N^2+6741N+9018)\langle R\rangle^9$	$-2520N^4\langle R\rangle^9$
10	$N(945N^4+42494N^3+249174N^2+532840N+774744)\langle R\rangle^{10}$	$945N^5\langle R\rangle^{10}$

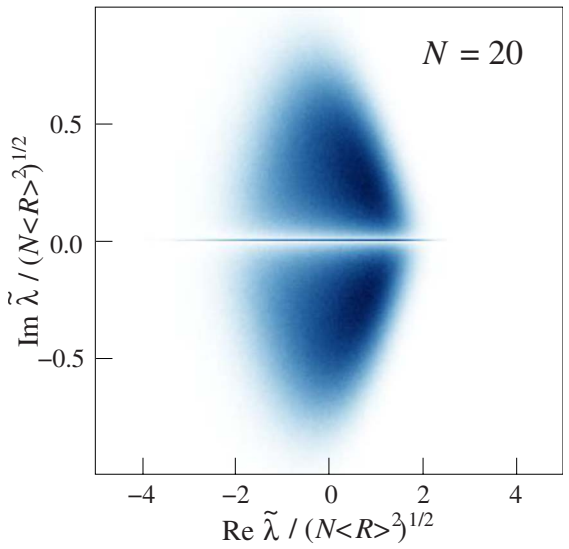

FIG. 4. (Color online) Scaled distribution function of nonzero eigenvalues $\tilde{\lambda}$ of shifted general rate matrices $\tilde{A}$ of dimension $N=20$. More specifically, a two-dimensional histogram with 500 $\times 500$ bins was populated for n_r matrices randomly chosen from the EGRE, with $n_r N=4\times 10^7$.

$$\rho_{\text{all}}(x,y)=\frac{1}{\pi N}\frac{\partial}{\partial z^*}\text{Tr}_{2N}\begin{pmatrix}0 & I\\ 0 & 0\end{pmatrix}\langle \mathcal{G}(0;z,z^*)\rangle, \tag{28}$$

where $z=x+iy$, the derivative with respect to z^* is to be taken with z fixed, and Tr_{2N} denotes the trace over a $2N\times 2N$ matrix. Using this representation, we show that for large N the eigenvalue density only depends on the second central moment $\langle \delta R^2\rangle$ of the distribution of rates A_{ij}. The proof is sketched in Appendix B. Edelman *et al.* [28] have conjectured that this is generically the case for asymmetric matrices.

We now present numerical results for $\rho(x,y)$ for the EGRE, as a function of the matrix dimensions N. As above, ρ_{all} contains all eigenvalues, whereas ρ excludes the exact zero. We will compare the results to the Ginibre ensemble of real asymmetric matrices with Gaussian distribution of components [Ginibre orthogonal ensemble (GinOE)] [21,28–33], which is the closest relative of the EGRE that has been studied in detail.

As observed above, the eigenvalues $\tilde{\lambda}$ of $\tilde{A}$ can be either real or form complex-conjugate pairs. The numerical simulations show that both types of eigenvalues indeed occur. A typical eigenvalue density is shown in Fig. 4 for $N=20$. We assume that the square root of the second pseudomoment, $\sqrt{\mu_2}=\sqrt{N\langle R\rangle^2}$, describes the typical width of the distribution and rescale the eigenvalue density accordingly. The real and complex eigenvalues are clearly visible. Here and in the following "complex" should be understood as "not real." Figure 4 already suggests that the distribution of nonzero eigenvalues of A becomes a narrow peak around $-N\langle R\rangle$ for large N, like for the ESRE. We return to this point below.

The question arises of what fraction f_{R} of the nonzero eigenvalues are real. For the GinOE, this fraction is known analytically [28]. (The probability of finding exactly N_{R} real eigenvalues for $N\times N$ matrices from the GinOE is also known [32].) Edelman *et al.* [28] derive various equivalent expressions for the expected number of real eigenvalues, $\langle N_{\text{R}}\rangle$, from which we obtain $f_{\text{R}}^{\text{GinOE}}=\langle N_{\text{R}}\rangle/N$. We here quote an expression in terms of the hypergeometric function ${}_2F_1$ [28]:

$$f_{\text{R}}^{\text{GinOE}}=\frac{1}{2N}+\sqrt{\frac{2}{\pi}}\frac{\Gamma(N+1/2)}{\Gamma(N+1)}{}_2F_1\left(1,-\frac{1}{2};N;\frac{1}{2}\right). \tag{29}$$

For large N, this becomes [28]

$$f_{\text{R}}^{\text{GinOE}}\cong\sqrt{\frac{2}{\pi N}}. \tag{30}$$

For the GinOE, the fraction of real eigenvalues thus asymptotically decays with a simple exponent of $-1/2$.

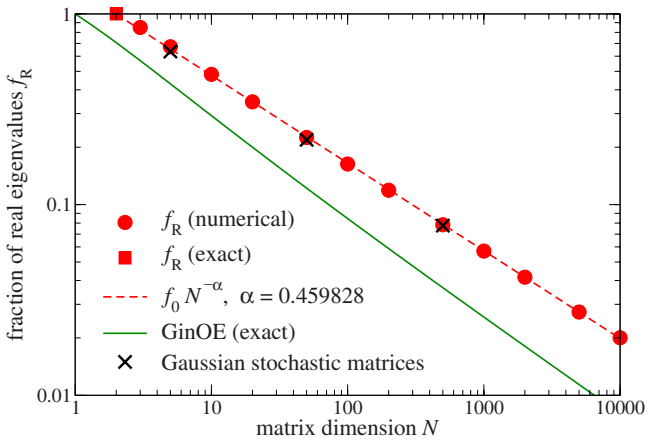

FIG. 5. (Color online) Fraction f_{R} of nonzero eigenvalues that are real, as a function of N for the EGRE. The solid circles denote numerical values obtained for n_r realizations with $n_r N=4\times 10^7$ for $N\leq 2000$, $n_r N=10^7$ for $N=5000$, and $n_r N=4\times 10^5$ for $N=10\,000$. The solid square represents the exact result $f_{\text{R}}=1$ for $N=2$. The dashed line denotes a power law $f_0 N^{-\alpha}$ fitted to the two points for $N=2000$ and $N=5000$. The solid line is the exact result for the GinOE [Eq. (29)]. The crosses denote numerical results for ensembles of rate matrices with Gaussian instead of exponential distribution of rates A_{ij}, $i\neq j$.

Figure 5 shows the fraction f_{R} as a function of N for the EGRE and for comparison the exact result for the GinOE. For $N=2$, f_{R} must be unity since the single nonzero eigenvalue cannot be a complex-conjugate pair. The results clearly differ from the GinOE and decay more slowly for large N. A fit of a power law $f_{\text{R}}\sim f_0 N^{-\alpha}$ to the data points for $N=2000$ and 5000 is also included in Fig. 5. We obtain $f_0\approx 1.37$ and $\alpha\approx 0.460$. The large-N behavior is inconsistent with the exponent 1/2 found for the GinOE. This is remarkable since all other scaling relations we have so far found, as well as the ones for the GinOE, only contain integer powers of $\sqrt{N}$. Physically, this means that the fraction of eigenvectors describing purely exponentially decaying deviations from the stationary state scales with a nontrivial power $-\alpha$ of the number of states.

To pinpoint the origin of the anomalous scaling, we have also evaluated f_{R} for ensembles of matrices of dimension

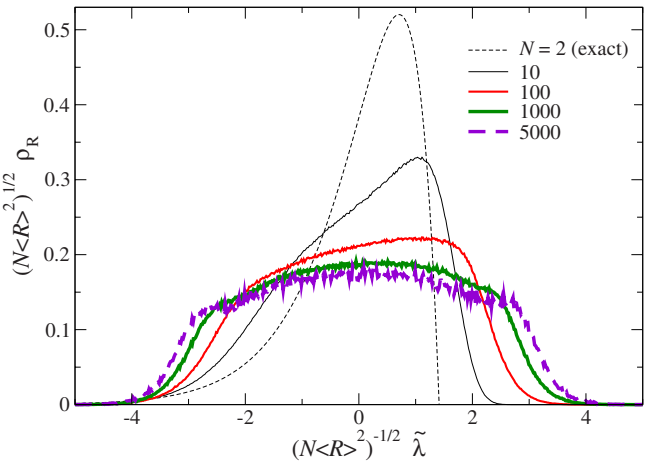

FIG. 6. (Color online) Scaled density of nonzero real eigenvalues of shifted general rate matrices $\tilde{A}$. The curve for $N=2$ is exact. The curves for $N=10$, 100, 1000, and 5000 are histograms with 500 bins for a total number $n_r N=4\times10^7$ (10^7) of eigenvalues (including complex ones) for $N\leq1000$ (5000) for matrices randomly chosen from the EGRE.

$N=5,50,500$ satisfying constraint (5) but with *Gaussian* distribution of rates A_{ij}, $i\neq j$. This is the asymmetric analog of the symmetric ensemble studied by Stäring *et al.* [24]. The results are shown as crosses in Fig. 5. They clearly approach the EGRE results for large N, not the GinOE. It is thus constraint (5) that leads to the anomalous scaling.

In the following, we will consider the real and complex eigenvalues separately. Figure 6 shows the density ρ_{R} of shifted real nonzero eigenvalues $\tilde{\lambda}$, normalized to unity and rescaled with the square root of the pseudomoment $\sqrt{\mu_2}=\sqrt{N\langle R\rangle^2}$, for $N=2$, 10, 100, 1000, and 5000. For $N=2$, the single nonzero eigenvalue is $\tilde{\lambda}=-\tilde{A}_{12}-\tilde{A}_{21}$. In the EGRE, its distribution function is $\rho_{\mathrm{R}}(\tilde{\lambda})=(2/\langle R\rangle-\tilde{\lambda}/\langle R\rangle^2)\exp(\tilde{\lambda}/\langle R\rangle-2)$ for $\tilde{\lambda}\leq2\langle R\rangle$ and zero otherwise. For the other values of N, Fig. 6 shows numerical results. The noise increases for large N not only because $n_r N$ was smaller for $N=5000$ but also because f_{R} decreases with increasing N. It is obvious that, however, the distribution for large N is quite different from the eigenvalue density for the ESRE (Fig. 1).

The distribution clearly becomes more symmetric for $N\to\infty$, as it must, since the large-N result only depends on the width of the distribution of rates A_{ij}. There is an indication that the distribution develops nonanalyticities with sudden changes in slope in the limit $N\to\infty$. This is not unexpected since the scaled distribution of real eigenvalues of the GinOE is uniform on the interval $[-1,1]$ and zero otherwise [28,33], and thus also shows nonanalyticities. Compared to the ESRE (Fig. 1), the convergence to the large-N limit is slower for the EGRE (Fig. 6). In fact, from Fig. 6 we cannot exclude the possibility that the width scales with an anomalous power of N, different from 1/2.

Turning to complex eigenvalues, we note that for large N nearly all eigenvalues belong to this class since the fraction f_{R} of real eigenvalues approaches zero. We plot their distribution function ρ_{C} in the complex plane for $N=100$ and 2000 in Fig. 7. The scaled distribution for $N=5000$ is virtually

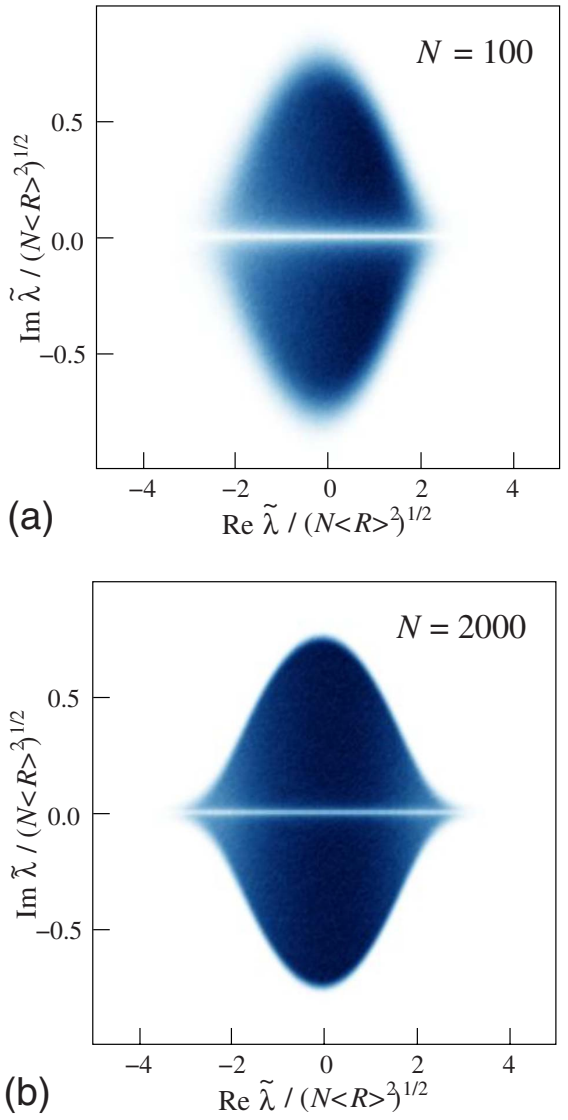

FIG. 7. (Color online) Scaled distribution function of complex eigenvalues $\tilde{\lambda}$ of shifted general rate matrices $\tilde{A}$ of dimensions (a) $N=100$ and (b) $N=2000$. Specifically, two-dimensional histograms with 500×500 bins were populated for n_r matrices randomly chosen from the EGRE, where $n_r N=4\times10^7$. Note the different scales of the axes.

indistinguishable from the one for $N=2000$. From Figs. 4 and 7, we see that the distribution becomes more symmetric with respect to inversion of the real part as N increases.

The widths of the distribution in the real direction, $\sqrt{\mu_{2,0}}$, and in the imaginary direction, $\sqrt{\mu_{0,2}}$ [see Eq. (25)] both scale with $\sqrt{N\langle R\rangle^2}$. This means that the typical decay rate is $\langle\lambda\rangle'=N\langle R\rangle$, whereas the typical oscillation frequency is of the order of $\sqrt{N}\langle R\rangle$. For large N it will thus be difficult to observe the oscillations.

It is instructive to compare the distribution to the one for the GinOE. For the GinOE, the distribution function ρ_{C} of complex eigenvalues for finite N has been obtained by Edelman [31] in terms of a finite sum of $N-1$ terms, which can be rewritten as a simple integral [33]. The distribution function ρ_{C} is found to contain a factor $|\mathrm{Im}\,\tilde{\lambda}|$, showing that the

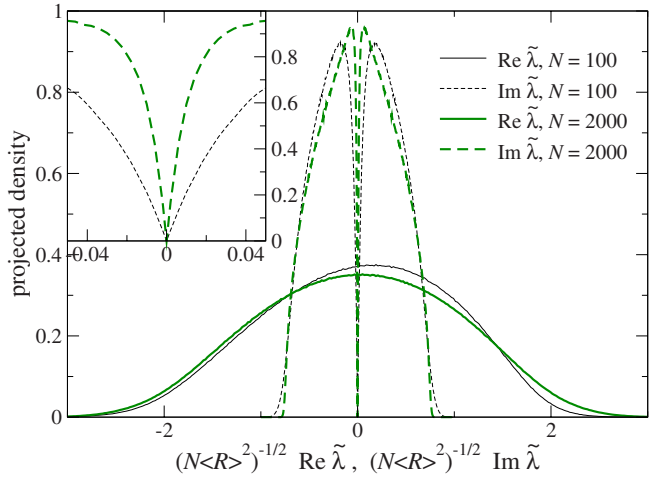

FIG. 8. (Color online) Scaled density of the real part (solid lines) and the imaginary part (dashed lines) of complex eigenvalues of shifted general rate matrices with $N=100$ and $N=2000$. The curves are projections of the data shown in Fig. 7 onto the real and imaginary axes. The inset shows the scaled density of the imaginary part around zero.

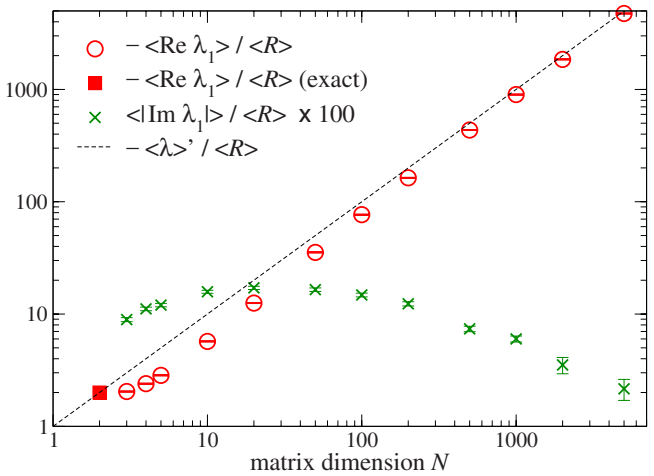

FIG. 9. (Color online) Typical real and imaginary parts of the eigenvalue belonging to the slowest nonstationary process, as functions of N. The open circles denote the average smallest in magnitude real part of eigenvalues, $\langle \mathrm{Re}\ \lambda_1\rangle$, of matrices from the EGRE. The data are numerical results for $n_r=5000$ (1000) realizations for $N\leq 1000$ ($N\geq 2000$). The crosses denote the average magnitude of the imaginary part of the same eigenvalues, $\langle|\mathrm{Im}\ \lambda_1|\rangle$, scaled $\times 100$. Error bars denoting the statistical errors are shown. The filled square denotes the exact result $\lambda_1=-2\langle R\rangle$ for $N=2$. The dashed line denotes the mean of nonzero eigenvalues, $-N\langle R\rangle$.

density goes to zero linearly for $\tilde{\lambda}$ approaching the real axis. Complex eigenvalues are thus repelled by the real axis with a characteristic exponents of unity. Figures 4 and 7 clearly show that complex eigenvalues are also repelled by the real axis for the EGRE. In Fig. 8 we plot the density of complex eigenvalues, projected onto the real and imaginary axes, for $N=100$ and $N=2000$. We observe that for the EGRE the complex eigenvalues are repelled by the real axis with the same exponent of unity. We note that the distribution of the real part of complex eigenvalues is distinct from both the distribution of real eigenvalues (Fig. 6) and the distribution of eigenvalues for the ESRE (Fig. 1).

For the GinOE, the scaled distribution approaches a uniform distribution on the unit disk in the complex plane for $N\to\infty$. This was conjectured by Girko [29] for an arbitrary distribution of components with zero mean and proven by Bai [30]. The EGRE result is clearly much more complicated. The histograms for various values of N suggest that the distribution function $\rho_{\mathbb{C}}$ does not become uniform in a bounded region for $N\to\infty$ although it does appear to develop nonanalyticities, which show up as high-contrast edges in Fig. 7(b).

We now return to the moments of the distribution function ρ of *all* nonzero eigenvalues of $\tilde{A}$. The moments μ_{mn} [Eq. (25)] and the pseudomoments μ_m [Eq. (24)] are related. This is easily seen for μ_2,

$$\mu_2 = \langle\tilde{\lambda}^2\rangle' = \langle(\mathrm{Re}\ \tilde{\lambda})^2 + 2i\ \mathrm{Re}\ \tilde{\lambda}\ \mathrm{Im}\ \tilde{\lambda} - (\mathrm{Im}\ \tilde{\lambda})^2\rangle. \quad (31)$$

Since the second term vanishes, we obtain $\mu_2=\mu_{2,0}-\mu_{0,2}$. Now $\mu_{2,0}$ contains contributions from the real and the complex eigenvalues while $\mu_{0,2}$ only depends on the complex eigenvalues. We can write

$$\mu_2 = f_{\mathbb{R}}\mu_2^{\mathbb{R}} + (1-f_{\mathbb{R}})\mu_{2,0}^{\mathbb{C}} - (1-f_{\mathbb{R}})\mu_{0,2}^{\mathbb{C}}, \quad (32)$$

where the superscript $\mathbb{R}$ or $\mathbb{C}$ refers to the moments of the distributions of real and complex eigenvalues, respectively. In the limit of large N we know that $f_{\mathbb{R}}\to 0$ and $\mu_2\cong N\langle R\rangle^2$. This means that the scaled distribution in the complex plane must be anisotropic: the width in the imaginary direction must be smaller by a value of the order of unity than in the real direction, unlike for the GinOE. This is seen in Fig. 7.

For arbitrary even m, the relation reads

$$\mu_m = \sum_{n=0\ \text{even}}^{m} (-1)^{n/2}\binom{m}{n}\mu_{m-n,n}$$

$$= f_{\mathbb{R}}\mu_m^{\mathbb{R}} + (1-f_{\mathbb{R}})\sum_{n=0\ \text{even}}^{m} (-1)^{n/2}\binom{m}{n}\mu_{m-n,n}^{\mathbb{C}}. \quad (33)$$

We recall that the μ_m for small m are known for all N, see Table IV. For large N, we have the asymptotically exact expression [Eq. (C8)], which can be written as $\mu_m \cong (m-1)!!N^{m/2}\langle R\rangle^m$. Hence, we find asymptotically exact sum rules for all even orders m.

To end this section, we again consider the slowest process. The dynamics at late times is typically governed by the eigenvalue λ_1 with the largest (smallest in magnitude) real part. In Fig. 9 we show the mean of the real part $\mathrm{Re}\ \lambda_1$ and of the magnitude of the imaginary part, $|\mathrm{Im}\ \lambda_1|$ for random matrices from the EGRE, as functions of N. The behavior of the real part, i.e., the rate, is very similar to the ESRE. Again, the slowest rate is consistent with the mean and width of the eigenvalue distribution $\rho(\lambda)$. The typical imaginary part of λ_1, i.e., the oscillation frequency, decreases for large N,

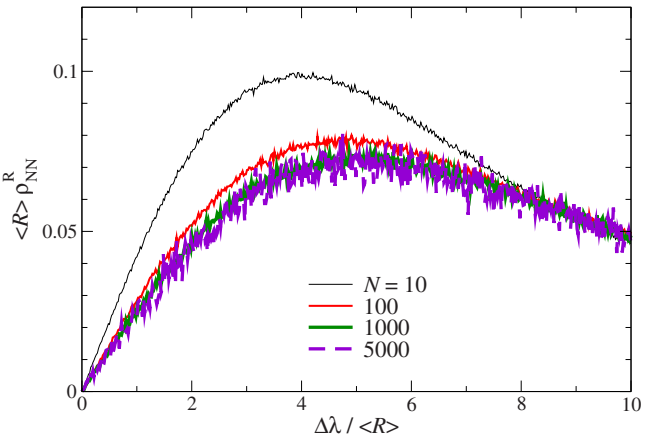

FIG. 10. (Color online) Distribution of nearest-neighbor separations $\Delta\lambda$ of nonzero real eigenvalues for the EGRE for $N=10$, 100, 1000, and 5000 for the same data sets as in Fig. 6. The axes are not rescaled with a power of N.

mainly because the probability of λ_1 being real increases. While the fraction of real eigenvalues approaches zero for large N, the eigenvalue with the largest real part becomes more likely to be real.

B. Eigenvalue correlations

The eigenvalue density for the EGRE is quite different from the GinOE. Like for the ESRE, we again ask whether the eigenvalue correlations are also different. We consider the real and complex eigenvalues separately. The main effect of correlations between real and complex eigenvalues is seen in Fig. 8: the complex eigenvalues are repelled by the real axis with a characteristic exponent of unity.

Figure 10 shows the distribution function $\rho^{\mathrm{R}}_{\mathrm{NN}}(\Delta\lambda)$ of separations of neighboring real eigenvalues. Note that the distribution is not rescaled with a power of N. The typical separation of real eigenvalues depends only weakly on N for large N for the EGRE, whereas it scales with $N^{-1/2}$ for the ESRE. This can be understood as follows: the expected number of real eigenvalues of a randomly chosen matrix is $Nf_{\mathrm{R}} \sim N^{1-\alpha}$ while the width of their distribution scales with $N^{1/2}\langle R\rangle$. Consequently, the typical nearest-neighbor separation should scale with $N^{\alpha-1/2}\langle R\rangle$. Since α is close to 1/2, we obtain a weak dependence on N. The dependence on separation $\Delta\lambda$ is again linear for small $\Delta\lambda$ though. Thus real eigenvalues repel each other with a characteristic exponent of unity, like for the GinOE [33].

In Figs. 11(a) and 11(b), we plot the distribution function $\rho^{\mathrm{C}}_{\mathrm{NN}}(\Delta\lambda)$ of complex differences of neighboring complex eigenvalues with positive imaginary part for $N=20$ and $N=2000$. More specifically, for each eigenvalue $\tilde{\lambda}$ with positive imaginary part, we determine the eigenvalue $\tilde{\lambda}'$ with positive imaginary part that minimizes $|\tilde{\lambda}'-\tilde{\lambda}|$. We then collect the complex differences $\Delta\lambda \equiv \tilde{\lambda}'-\tilde{\lambda}$ of all such pairs in a two-dimensional histogram. The eigenvalues with negative imaginary part just form a mirror image. Correlations between eigenvalues with positive and negative imaginary parts are dominated by their repulsion by the real axis and a δ function from complex-conjugate pairs and are not considered further.

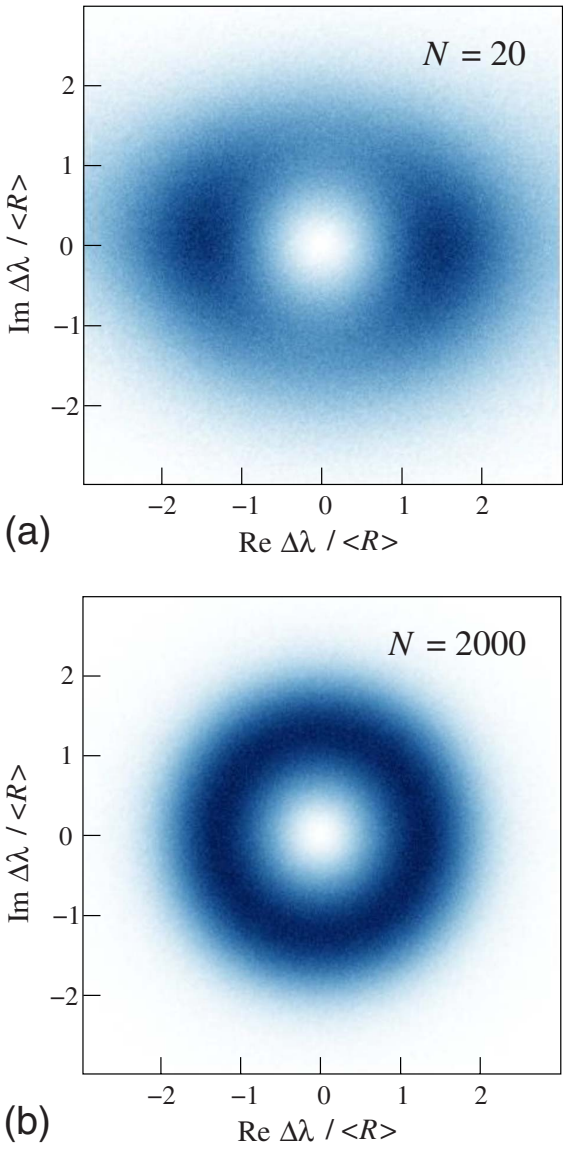

FIG. 11. (Color online) Distribution function of complex differences $\Delta\lambda$ of neighboring eigenvalues with positive imaginary part for the EGRE for (a) $N=20$ and (b) $N=2000$.

Since the fraction of complex eigenvalues approaches unity for $N\to\infty$, the number of complex eigenvalues of a chosen matrix scales with N. The widths of the distribution in both the real and the imaginary directions scale with $\sqrt{N}$, see Fig. 7. The typical nearest-neighbor distance should thus approach a constant for large N. This is indeed seen in Fig. 11.

We observe that the distribution of differences becomes rotationally symmetric for large N. This is perhaps surprising since the distribution of the eigenvalues themselves is far from symmetric, see Fig. 7. Also, small differences are suppressed, i.e., the eigenvalues repel each other. To find the characteristic exponent, we plot the distribution of the magnitudes $|\Delta\lambda|=|\tilde{\lambda}'-\tilde{\lambda}|$ of differences of neighboring eigenval-

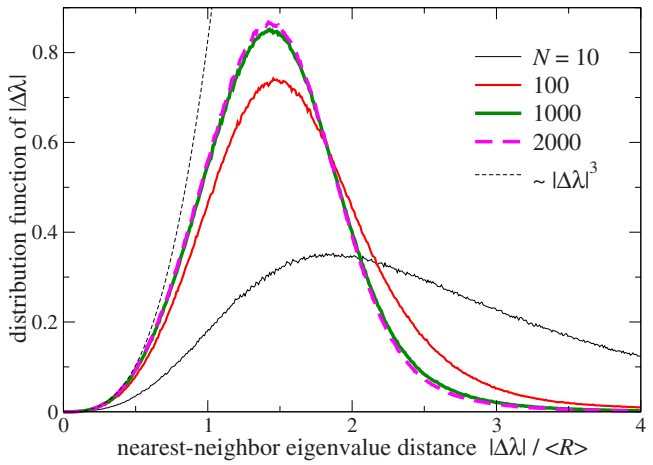

FIG. 12. (Color online) Distribution function of nearest-neighbor distances $|\Delta\lambda|$ for various values of N. The dashed curve shows a power law $\propto|\Delta\lambda|^3$.

ues in Fig. 12. We observe that the distribution behaves like $|\Delta\lambda|^3$ for small $|\Delta\lambda|$. Together with the rotational symmetry this implies that the two-dimensional distribution in the complex plane [Fig. 11(b)] approaches zero like $|\Delta\lambda|^2$. The exponent of two is the same as for the GinOE [33]. We conclude that constraint (5) and the exponential distribution of rates in the EGRE do not change the repulsion of neighboring eigenvalues compared to the GinOE while the eigenvalue density is very different. The origin of this is likely the same as to the ESRE: the correlations are governed by "local" properties of the joint distribution function of eigenvalues, which are not strongly affected by the constraint.

IV. CONCLUSIONS

We have applied RMT to the transition-rate matrix A, i.e., the matrix of coefficients in the Pauli master equation [Eq. (3)]. This allows us to obtain statistical properties of the spectrum, in analogy to RMT for Hamiltonians. For the master equation, the eigenvalues describe the decay, and, in the case of complex eigenvalues, the superimposed oscillations, of probability eigenvectors.

The resulting random-matrix ensembles are different from the standard ensembles for Hamiltonians since A is real but in general not symmetric and since the conservation of probability imposes the constraint $\Sigma_i A_{ij}=0$ for all j [Eq. (5)]. Although this constraint represents only N conditions for of the order of N^2 matrix components, its consequences persist for large N.

A further difference to the standard ensembles is that the off-diagonal components of the rate matrix represent rates and thus must be non-negative. We have assumed an exponential distribution. The results in the large-N limit are found to be independent of the distribution of rates though.

We have considered both symmetric and general asymmetric rate matrices. The first case corresponds to systems where the rates for transitions from any state i to any other state j and from j to i are identical. In the second case, these rates are assumed to be independent. In both cases, all nonzero eigenvalues form a narrow distribution of width proportional to $\sqrt{N}$ around their mean, $-N\langle R\rangle$, where $\langle R\rangle$ is the average transition rate. Thus for not too small N, nearly all deviations from the stationary state decay on the same time scale $1/N\langle R\rangle$. For both cases, we have found that the slowest nonstationary state, which dominates the dynamics at late times, typically also decays on the same time scale. We have derived exact expressions for the expectation values of mth powers of the nonzero eigenvalues, for small m, for both cases.

For *symmetric* rate matrices, the density of eigenvalues has been studied numerically as a function of N and found to approach the same limiting form for $N\to\infty$ as obtained earlier for Gaussian and two-valued distributions [22–24] but very different from the semicircle law for the GOE [16,19]. This difference is due to constraint (5). On the other hand, the correlations between eigenvalues are dominated by a repulsion with a characteristic exponent of unity, as for the GOE.

For *general* rate matrices, we have numerically studied the eigenvalue density in the complex plane as a function of N. For large N, it approaches a nontrivial distribution different from the disk found for the GinOE [29,30]. Interestingly, the fraction of nonzero eigenvalues that are real decays as $N^{-\alpha}$ with an anomalous exponent $\alpha\approx 0.460$, unlike for the GinOE, where $\alpha=1/2$. Thus the fraction of eigenvectors describing purely exponentially decaying deviations from the stationary state scales with a nontrivial power of the number of possible states. Both the nontrivial distribution and the anomalous scaling for large N are due to constraint (5). The density of real eigenvalues is also different from the GinOE. We have obtained simple analytical results for the expectation values $\langle(\lambda-\langle\lambda\rangle')^m\rangle'=(m-1)!!(N\langle\delta R^2\rangle)^{m/2}$ of *all* even powers of shifted nonzero eigenvalues in the limit of large N. Interestingly, they agree with the central moments of a real Gaussian distribution. The central moments of the eigenvalue density in the complex plane are shown to satisfy exact sum rules involving these expectation values.

Correlations between eigenvalues are found to agree with the GinOE: real eigenvalues repel each other with an exponent of unity while complex eigenvalues are repelled by the real axis with an exponent of unity and by each other with an exponent of two.

In view of the power of RMT for Hamiltonians, we hope that this approach will also benefit our understanding of complex stochastic processes. Comparisons with real processes are now called for.

APPENDIX A: LARGE-N LIMIT FOR SYMMETRIC RATE MATRICES

In the limit of large N, the density of eigenvalues $\tilde{\lambda}$ of $\tilde{A}$ only depends on the second moment $\langle\delta R^2\rangle$ of the distribution of components $\tilde{A}_{ij}$, $i\neq j$, for any distribution function of $\tilde{A}_{ij}$, as long as all its central moments exist. In this appendix, we sketch the proof of this statement.

The eigenvalue density is given by Eq. (18). In the expansion of the geometric series for the resolvent [26],

$$\langle \tilde{G}(z) \rangle = \sum_{n=0}^{\infty} \frac{\mathrm{Tr}\langle \tilde{A}^n \rangle}{z^{n+1}}, \tag{A1}$$

the $n=0$ term is independent of the distribution of $\tilde{A}_{ij}$, while the $n=1$ term vanishes. Since $\Sigma_i \langle \tilde{A}^n \rangle_{ij} = 0$ for $n \geq 1$ we can write

$$\langle \tilde{G}(z) \rangle = \frac{1}{z} - \sum_{n=2}^{\infty} \frac{1}{z^{n+1}} \sum_{ij, i \neq j} \langle \tilde{A}^n \rangle_{ij} = \frac{1}{z} - \sum_{n=2}^{\infty} \frac{1}{z^{n+1}} \sum_{ij, i \neq j} \sum_{k_1, k_2, \ldots} \langle \tilde{A}_{ik_1} \tilde{A}_{k_1 k_2} \cdots \tilde{A}_{k_{n-1} j} \rangle. \tag{A2}$$

We now introduce a diagrammatic representation for the expectation values $\langle \tilde{A}^m \rangle_{ij}$, $i \neq j$:

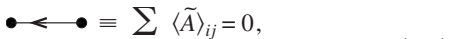

$$\equiv \sum_{ij, i \neq j} \langle \tilde{A} \rangle_{ij} = 0, \tag{A3}$$

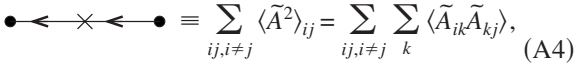

$$\equiv \sum_{ij, i \neq j} \langle \tilde{A}^2 \rangle_{ij} = \sum_{ij, i \neq j} \sum_{k} \langle \tilde{A}_{ik} \tilde{A}_{kj} \rangle, \tag{A4}$$

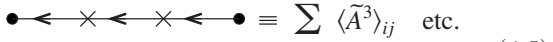

$$\equiv \sum_{ij, i \neq j} \langle \tilde{A}^3 \rangle_{ij} \quad \text{etc.} \tag{A5}$$

Here, an arrow represents a factor of $\tilde{A}$, a vertex (filled circle or cross) represents a matrix index, and all indices are summed over $1, \ldots, N$, subject to the constraint that indices corresponding to filled circles are distinct. Vertices drawn as crosses do not imply any constraint.

In Eq. (A2), we now decompose the sums over indices into terms with equal and distinct indices. For equal indices we attach the arrows to the same filled-circle vertex, whereas distinct indices are denoted by distinct filled-circle vertices. For example,

$\sum_{ij, i \neq j} \langle \tilde{A}^2 \rangle_{ij} =$ 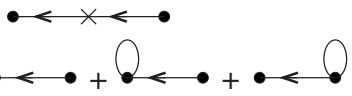

(A6)

The constraint $\tilde{A}_{jj} = -\Sigma_{i \neq j} \tilde{A}_{ij}$ assumes the form

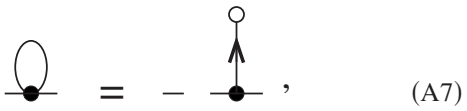

(A7)

where the open circle denotes an index that is different from the one connected to it but not otherwise constrained. Applying this rule to all terms, we obtain open-circle vertices, which we dispose of by again distinguishing between equal and distinct indices. For example,

$\sum_{ij, i \neq j} \langle \tilde{A}^2 \rangle_{ij} =$ 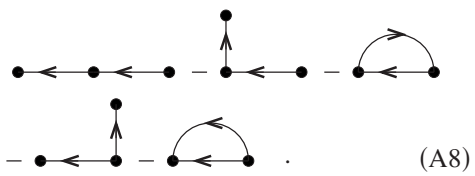

(A8)

We have achieved that factors of $\tilde{A}$ with two equal indices are no longer present and that all indices to be summed over are distinct.

Since different off-diagonal components $\tilde{A}_{ij}$ are independent, except for $\tilde{A}_{ji} = \tilde{A}_{ij}$, the expectation value of each term decays into a product of expectation values of powers of components, $\langle \delta R^m \rangle \equiv \langle (\tilde{A}_{ij})^m \rangle$. The corresponding diagrams are of the forms

$= 0,$ (A9)

(A10)

(A11)

Finally, any term containing m vertices obtains a factor $N(N-1)(N-2)\cdots(N-m+1)$ from the sum over distinct indices. In the limit of large N this becomes N^m.

We conclude that at any order $n \geq 2$ in Eq. (A2), the largest terms for large N are the nonvanishing ones with the maximum number of vertices. Note that the diagrams generated by this procedure are always connected. Diagrams containing single arrows connecting two vertices vanish because of Eq. (A9). For even n, the maximum number of vertices is $n/2+1$, which is obtained if all connections are double arrows. In this case the contribution is proportional to $N^{n/2+1} \langle \delta R^2 \rangle^{n/2}$. The next smaller terms have two triple arrows and contribute $\propto N^{n/2} \langle \delta R^2 \rangle^{n/2-3} \langle \delta R^3 \rangle^2$. For odd n, the largest terms have one triple arrow and all other connections are double arrows. Their contribution is proportional to $N^{n/2+1/2} \langle \delta R^2 \rangle^{n/2-3/2} \langle \delta R^3 \rangle$.

Since Eq. (18) contains an explicit factor of $1/N$, the leading contributions to the density scale as $N^{n/2}$ ($N^{n/2-1/2}$) for even (odd) n. If we rescale the density so that the width approaches a constant, the odd terms in expansion (A2) vanish like $N^{-1/2}$, showing that the rescaled density approaches an even function. Furthermore, the leading even terms only depend on the second moment $\langle \delta R^2 \rangle$, which is what we set out to prove.

Rewriting Eq. (A1) in terms of the moments μ_n,

$$\langle \tilde{G}(z) \rangle = \frac{1}{z} + (N-1) \sum_{n=2}^{\infty} \frac{\mu_n}{z^{n+1}}, \tag{A12}$$

we see that the terms of order n contribute exclusively to the moment μ_n. The result proven here is consistent with the calculated moments in Table I.

APPENDIX B: LARGE-N LIMIT FOR GENERAL RATE MATRICES

For ensembles of general asymmetric rate matrices, it is also true that the density of eigenvalues only depends on the second moment $\langle \delta R^2 \rangle$ for large N. We here sketch the proof of this assertion.

The distribution of eigenvalues in the complex plane is given by Eqs. (26)–(28). We define

$$g(\eta;z,z^*) \equiv \mathrm{Tr}_{2N}\begin{pmatrix} 0 & I \\ 0 & 0 \end{pmatrix}\langle \mathcal{G}(0;z,z^*)\rangle, \tag{B1}$$

so that $\rho_{\mathrm{all}}(x,y)=(1/\pi N)\partial g(0;z,z^*)/\partial z^*$ and expand the resolvent,

$$g(\eta;z,z^*) = \sum_{n \text{ odd}} \frac{1}{\eta^{n+1}} \mathrm{Tr}\langle [(\tilde{A}^T - z^* I)(\tilde{A} - zI)]^{(n-1)/2}(\tilde{A}^T - z^* I)\rangle. \tag{B2}$$

Expanding the products, we obtain a linear combination of expressions of the form $\mathrm{Tr}\langle \cdots \tilde{A}^T \cdots \tilde{A} \cdots \rangle$ containing any number of factors $\tilde{A}^T$ and $\tilde{A}$ in any order. Now the arguments of Appendix A go through with few changes. We can group the terms according to the total order m of $\tilde{A}$ and $\tilde{A}^T$. The term of order zero is independent of the distribution of $\tilde{A}_{ij}$. The terms of first order are $\mathrm{Tr}\langle \tilde{A}\rangle = \mathrm{Tr}\langle \tilde{A}^T\rangle = 0$. In all other terms we can use cyclic permutation under the trace and the identity $\mathrm{Tr}\, B^T = \mathrm{Tr}\, B$ to make sure that a factor $\tilde{A}$ and not $\tilde{A}^T$ is appearing first under the trace. We can then use Eq. (5) to write $\mathrm{Tr}\langle \tilde{A} \cdots \rangle = -\Sigma_{ij,i\neq j}\langle \tilde{A}_{ij} \cdots \rangle_{ij}$.

Now we can apply the diagrammatics of Appendix A. $(\tilde{A}^T)_{ij} = \tilde{A}_{ji}$ is drawn as an arrow pointing in the opposite direction. In the evaluation of expectation values corresponding to Eqs. (A10) and (A11), we have to take into account that $\tilde{A}_{ij}$ and $\tilde{A}_{ji}$ are now independent so that we instead have

= 0, (B3)


$= \langle \delta R^2 \rangle$, (B4)


= 0, (B5)


$= \langle \delta R^3 \rangle$, (B6)

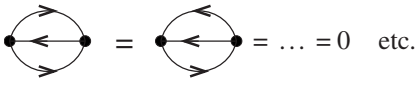
= … = 0 etc. (B7)

We note that all terms of the same order m in Eq. (B2) have the same sign and thus cannot cancel. We thus find that to any order m the leading terms in Eq. (B2) for large N have the same form as for symmetric matrices. In particular, for even m the leading term in the density $\rho(x,y)$ scales with $N^{m/2}\langle \delta R^2\rangle^{m/2}$ and the odd terms scale with a lower power of N. Finally, it is conceivable that taking the derivative of $g(0;z,z^*)$ with respect to z^* in order to obtain the density could remove the leading-N term. This is not the case since for any even order $m \geq 2$ there is at least a contribution from $m=n-1$ in Eq. (B2), which is linear in z^*.

APPENDIX C: PSEUDOMOMENTS FOR THE EGRE

In this appendix, we use the diagrammatics of Appendix A to calculate the pseudomoments

$$\mu_m = \langle \tilde{\lambda}^m \rangle' = \frac{1}{N-1}\mathrm{Tr}\langle \tilde{A}^m \rangle, \tag{C1}$$

$m \geq 2$, to leading order for large N for the EGRE. Appendix B shows that for large N only the even pseudomoments are relevant. We write

$$\mu_m = -\frac{1}{N-1}\sum_{ij,i\neq j}\langle \tilde{A}^m \rangle_{ij} = -\frac{1}{N-1}\sum_{ij,i\neq j}\sum_{k_1,k_2,\ldots}\langle \tilde{A}_{ik_1}\tilde{A}_{k_1k_2}\cdots\tilde{A}_{k_{m-1}j}\rangle. \tag{C2}$$

It was shown in Appendix B that for large N the distribution of $\tilde{A}_{ij}$ only enters through its second moment $\langle \delta R^2\rangle$. We decompose all terms into a sum of contributions with equal or distinct indices, see Eq. (A6). For each term, some or none of the indices in $\{i,k_1,k_2,\ldots,k_{m-1},j\}$ are equal. Contributions for which two equal indices are separated by other distinct indices in this string correspond to diagrams of the type


, (C3)

and are of lower order in N. All remaining diagrams are of the form of chains leading from j to i with any number of single-vertex loops $(\tilde{A}_{kk})$ decorating the vertices. We call these single-vertex loops "leaves."

Next, we prove


$\cong 0$, (C4)

for $N \to \infty$, where the left-most vertex in the first term carries $l \geq 1$ leaves while the second vertex in the second term carries $l-1 \geq 0$ leaves. The shaded circle is an arbitrary diagram part. The proof proceeds as follows: Applying rule (A7), we obtain

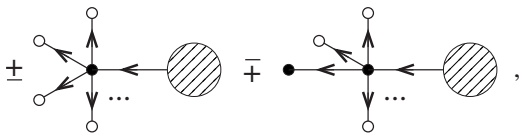
, (C5)

with the upper (lower) signs for even (odd) l. In the leading large-N term, all connections must be of the form of two arrows pointing in the same direction, as in Eq. (B4). This is only possible if we pair up the open-circle vertices among themselves, not with any vertices in the right-hand part of the diagrams. This requires l to be even. Furthermore, for the first diagram there are $(l-1)!!$ ways to partition l leaves into pairs. For the second diagram there are $l-1$ ways to pair one of the leaves with the leftmost vertex and $(l-3)!!$ ways to partition the remaining $l-2$ leaves into pairs. With these factors we obtain

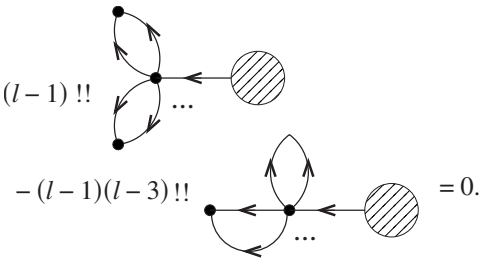

(C6)

All diagrams of leading order in N are of the form of one of the two diagrams in Eq. (C4). Thus all diagrams cancel, except if only one of the two forms exists. This is only the case for

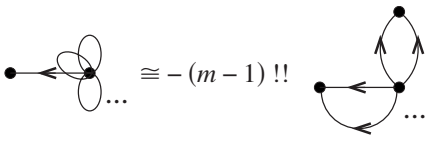

$$\cong -(m-1)!!\, N^{m/2+1}\langle \delta R^2\rangle^{m/2}, \tag{C7}$$

since its partner would contain only a single vertex, which is excluded by $i \neq j$.

With the prefactor from Eq. (C2), we obtain

$$\mu_m \cong (m-1)!!\, N^{m/2}\langle \delta R^2\rangle^{m/2}. \tag{C8}$$

[1] A. E. Siegman, *Lasers* (University Science Books, Sausalito, 1986).
[2] S. Alexander, J. Bernasconi, W. R. Schneider, and R. Orbach, Rev. Mod. Phys. **53**, 175 (1981).
[3] J. E. Carroll, *Rate Equations in Semiconductor Electronics* (Cambridge University Press, Cambridge, England, 2002).
[4] L. I. Glazman and K. A. Matveev, Pis'ma Zh. Eksp. Teor. Fiz. **48**, 403 (1988) [JETP Lett. **48**, 445 (1988)].
[5] M. Galperin, M. A. Ratner, and A. Nitzan, J. Phys.: Condens. Matter **19**, 103201 (2007).
[6] R. K. Wangsness and F. Bloch, Phys. Rev. **89**, 728 (1953); F. Bloch, *ibid.* **105**, 1206 (1957).
[7] A. G. Redfield, Adv. Magn. Reson. **1**, 1 (1965).
[8] M. Tokuyama and H. Mori, Prog. Theor. Phys. **54**, 918 (1975); **55**, 411 (1976).
[9] H.-P. Breuer and F. Petruccione, *The Theory of Open Quantum Systems* (Oxford University Press, Oxford, 2002).
[10] C. Timm, Phys. Rev. B **77**, 195416 (2008).
[11] C. Timm, Phys. Rev. B **76**, 014421 (2007).
[12] A. Berman and R. J. Plemmons, *Non-negative Matrices in the Mathematical Sciences* (Academic Press, New York, 1979).
[13] J. M. van den Hof, Ph.D. thesis (unpublished); http://irs.ub.rug.nl/ppn/152829512
[14] O. Perron, Math. Ann. **64**, 248 (1907).
[15] G. Frobenius, *Über Matrizen aus nicht negativen Elementen* (Sitzungsber. Preuss. Akad. Wiss., Berlin, 1912), p. 456.
[16] E. P. Wigner, in *Proceedings of the Canadian Mathematical Congress* (University of Toronto, Toronto, 1957), p. 174; reprinted in C. E. Porter, *Statistical Theories of Spectra: Fluctuations* (Academic Press, New York, 1965), p. 188; E. P. Wigner, SIAM Rev. **9**, 1 (1967).
[17] C. W. J. Beenakker, Rev. Mod. Phys. **69**, 731 (1997).
[18] T. Guhr, A. Müller-Groeling, and H. A. Weidenmüller, Phys. Rep. **299**, 189 (1998).
[19] M. L. Mehta, *Random Matrices*, 3rd ed. (Elsevier, Amsterdam, 2004).
[20] A. Amir, Y. Oreg, and Y. Imry, Phys. Rev. B **77**, 165207 (2008), also apply RMT to stochastic equation (3). In their approach, the quantities taking the place of our P_i are the deviations of occupation numbers of sites in a random system from the stationary state. Linearization for small deviations leads to Eq. (3). The distribution function of matrices studied by Amir *et al.* is completely different from Eq. (8) and, in particular, the rates A_{ij} are not independent. This leads to different results for the eigenvalue spectrum.
[21] J. Ginibre, J. Math. Phys. **6**, 440 (1965).
[22] A. J. Bray and G. J. Rodgers, Phys. Rev. B **38**, 11461 (1988).
[23] Y. V. Fyodorov, J. Phys. A **32**, 7429 (1999).
[24] J. Stäring, B. Mehlig, Y. V. Fyodorov, and J. M. Luck, Phys. Rev. E **67**, 047101 (2003).
[25] *Mathematica, vers. 6.0* (Wolfram Research, Champaign, 2007).
[26] M. A. Stephanov, J. J. M. Verbaarschot, and T. Wettig, in *Wiley Encyclopedia of Electrical and Electronics Engineering, Supplement 1*, edited by J. G. Webster (Wiley, New York, 2001).
[27] J. Feinberg, J. Phys. A **39**, 10029 (2006).
[28] A. Edelman, E. Kostlan, and M. Shub, J. Am. Math. Soc. **7**, 247 (1994).
[29] V. L. Girko, Theor. Probab. Appl. **29**, 694 (1985).
[30] Z. D. Bai, Ann. Probab. **25**, 494 (1997).
[31] A. Edelman, J. Multivariate Anal. **60**, 203 (1997).
[32] E. Kanzieper and G. Akemann, Phys. Rev. Lett. **95**, 230201 (2005).
[33] H.-J. Sommers and W. Wieczorek, J. Phys. A: Math. Theor. **41**, 405003 (2008).